RGSA – Revista de Gestão Social e Ambiental
ISSN: 1981-982X
Submission date: 08/12/2024
Acceptance date: 10/14/2024
DOI: https://doi.org/10.24857/rgsa.v18n11-204
Organization: Interinstitutional Scientific Committee
Chief Editor: Ana Carolina Messias de Souza Ferreira da Costa
Assessment: Double Blind Review pelo SEER/OJS

MAIN HEAT TRANSFER MECHANISMS IN *HOT STAMPING* PROCESSES: A REVIEW

Rafael Pandolfo da Rocha[1]
Matheus Henrique Riffel[2]
André Rosiak[3]
Lirio Schaeffer[4]

ABSTRACT

Objectives: The article reviews heat transfer mechanisms in the hot stamping process, highlighting models to calculate the interfacial heat transfer coefficient (IHTC), crucial for optimizing the cooling and quality of formed products.

Theoretical Framework: In hot stamping of high-strength steels, the IHTC is affected by variables such as contact pressure, roughness and temperature. Cooling efficiency directly impacts the temperature distribution and martensitic microstructure of the material, essential for structural strength.

Method: The review compares IHTC calculation methods, such as inverse heat conduction analysis and Newton's law of cooling, detailing the convection, radiation and conduction mechanisms at each stage of the process: transfer, positioning and forming.

Results and Discussion: The inverse heat conduction analysis proved to be the most accurate for determining the IHTC, compared to the finite element method (FEM). The study suggests that efficient cooling channels and high conductivity materials in the matrix reduce cooling time and improve the quality of the final product.

Research Implications: Findings provide a basis for improving thermal management in hot stamping, reducing cycle time and increasing productivity.

Originality/Value: This work contributes a comprehensive reference on IHTC, assisting researchers and engineers in optimizing heat transfer and production efficiency in the manufacture of automotive components.

Keywords: Hot Stamping, Interfacial Heat Transfer Coefficient, Heat Transfer Model, Conformable Cooling Channels.

PRINCIPAIS MECANISMOS DE TRANSFERÊNCIA DE CALOR EM PROCESSOS DE *HOT STAMPING*: UMA REVISÃO

RESUMO

Objetivos: O artigo revisa mecanismos de transferência de calor no processo de estampagem a quente, destacando modelos para calcular o coeficiente de transferência de calor interfacial (IHTC), crucial para otimizar o resfriamento e a qualidade dos produtos conformados.

[1] Universidade Federal do Rio Grande do Sul, Porto Alegre, Rio Grande do Sul, Brazil.
E-mail: rafel.pandolfo@ufrgs.br Orcid: https://orcid.org/0009-0004-7835-5159
[2] Universidade Federal do Rio Grande do Sul, Porto Alegre, Rio Grande do Sul, Brazil.
E-mail: matheus.riffel@ufrgs.br Orcid: https://orcid.org/0009-0009-4639-0431
[3] Universidade Federal do Rio Grande do Sul, Porto Alegre, Rio Grande do Sul, Brazil.
E-mail: andre.rosiak@ufrgs.br Orcid: https://orcid.org/0000-0002-7162-5169
[4] Universidade Tecnica de Aachen, Aachen, Renânia do Norte-Vestfália; Alemanha.
E-mail: 00002781@ufrgs.br Orcid: https://orcid.org/0000-0002-3427-2405

Quadro Teórico: Na estampagem a quente de aços de alta resistência, o IHTC é afetado por variáveis como pressão de contato, rugosidade e temperatura. A eficiência do resfriamento impacta diretamente a distribuição de temperatura e a microestrutura martensítica do material, essencial para resistência estrutural.

Método: A revisão compara métodos de cálculo do IHTC, como a análise de condução inversa de calor e a lei de resfriamento de Newton, detalhando os mecanismos de convecção, radiação e condução em cada etapa do processo: transferência, posicionamento e conformação.

Resultados e Discussão: A análise inversa de condução de calor mostrou-se a mais precisa para determinar o IHTC, em comparação ao método de elementos finitos (FEM). O estudo sugere que canais de resfriamento eficientes e materiais de alta condutividade na matriz reduzem o tempo de resfriamento e melhoram a qualidade do produto final.

Implicações da Pesquisa: Os achados fornecem uma base para aprimorar o gerenciamento térmico em estampagem a quente, reduzindo o tempo de ciclo e aumentando a produtividade.

Originalidade/Valor: Este trabalho contribui com uma referência abrangente sobre o IHTC, auxiliando pesquisadores e engenheiros na otimização da transferência de calor e na eficiência produtiva na fabricação de componentes automotivos.

Palavras-chave: Hot Stamping, Coeficiente de Transferência de Calor Interfacial, Modelo de Transferência de Calor, Canais Conformáveis de Resfriamento.

PRINCIPALES MECANISMOS DE TRANSFERENCIA DE CALOR EN PROCESOS DE ESTAMPACIÓN EN CALIENTE: UNA REVISIÓN

RESUMEN

Objetivos: El artículo revisa los mecanismos de transferencia de calor en el proceso de estampación en caliente, destacando modelos para calcular el coeficiente de transferencia de calor interfacial (IHTC), crucial para optimizar el enfriamiento y la calidad de los productos formados.

Marco Teórico: En la estampación en caliente de aceros de alta resistencia, el IHTC se ve afectado por variables como presión de contacto, rugosidad y temperatura. La eficiencia del enfriamiento afecta directamente la distribución de la temperatura y la microestructura martensítica del material, esencial para la resistencia estructural.

Método: La revisión compara los métodos de cálculo del IHTC, como el análisis de conducción inversa de calor y la ley de enfriamiento de Newton, detallando los mecanismos de convección, radiación y conducción en cada etapa del proceso: transferencia, posicionamiento y conformación.

Resultados y Discusión: El análisis de conducción de calor inversa demostró ser el más preciso para determinar el IHTC, en comparación con el método de elementos finitos (FEM). El estudio sugiere que los canales de enfriamiento eficientes y los materiales de alta conductividad en la matriz reducen el tiempo de enfriamiento y mejoran la calidad del producto final.

Implicaciones de la investigación: Los hallazgos proporcionan una base para mejorar la gestión térmica en el estampado en caliente, reducir el tiempo del ciclo y aumentar la productividad.

Originalidad/Valor: este trabajo aporta una referencia completa sobre IHTC, ayudando a investigadores e ingenieros a optimizar la transferencia de calor y la eficiencia de producción en la fabricación de componentes automotrices.

Palabras clave: Estampación en Caliente, Coeficiente de Transferencia de Calor Interfacial, Modelo de Transferencia de Calor, Canales de Enfriamiento Conformables.

1 INTRODUCTION

The hot-stamping process is carried out by heating microbonded boron steel sheets, such as 22MnB5, at temperatures above 900°C, for completely uniform austenitization. Subsequently, the generatrices are transferred to water or nitrogen cooling matrices for simultaneous execution of the stamping and tempering stages, with cooling rates above 27 °C/s, which forms a fully martensitic microstructure in the final component, with a resistance limit in the range of 1500 MPa (Figure 1). Turetta (2006) investigated the conformability of 22MnB5 in hot stamping operations. Karbasian and Tekkaya (2010) further revised the thermal, mechanical, microstructural and technological fields of this forming process. Hot stamped high strength steel parts have the advantages of high strength, high hardness, little elastic return and significant weight reduction, which makes hot stamping the best process to produce complex automotive structural components such as A pillars, B pillars and side impact beams etc.

During the forming and tempering stages, heat is transferred from the *blank* under high temperature to the matrices kept at low temperature. The interfacial heat transfer coefficient (IHTC) between the blank and the matrix is an important thermophysical parameter indicating heat transferability. The IHTC directly impacts the temperature distribution in the blank and consequently affects the mechanical property and microstructure of the final part (Figure 2). The understanding of the IHTC is indispensable for the configuration of numerical simulation (finite element analysis), in order to obtain reliable results about the *Hot Stamping* processes (Zhao, 2015).

Figure 1

Temperature behavior during the hot stamping process.

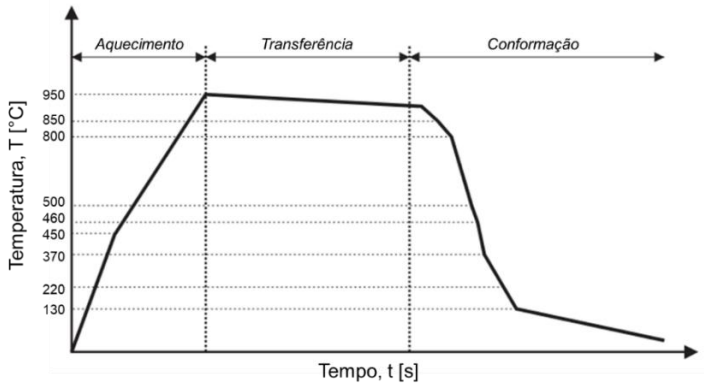

Source: Karbasian, 2010.

Research efforts have been made to develop models to design and optimize the tool cooling system in order to increase the cooling speed and achieve a more uniform temperature distribution of the surfaces of the conformed parts (Steinbeiss, 2007; Shan, 2010; Liu, 2013; Lim, 2014; Zamri, 2015). The models developed and optimization methods are useful in determining the structural parameters of the cooling system that maximize heat transfer. However, some of the models are computationally intensive and not applicable to tools with complex geometry. Another strategy involves the use of tools materials with high thermal conductivity (Altan 2012; Escher 2015; Ghiotti 2016). On the other hand, some of the materials are expensive and are still being developed.

In the theory of heat transfer, the IHTC is a parameter to describe the heat transfer between interfaces and is also considered as a constant value under ideal conditions (Chang, 2016). However, an ideal condition is difficult to achieve in practice and the IHTC is influenced by many factors Ikeuchi and Yanagimoto (2011) demonstrated that contact pressure, blank and matrix temperature, surface roughness and thermophysical properties of the material influence in the IHTC. Abdulhay (2012) obtained thermal contact resistance at different locations of a U-shaped end part, with contact pressure ranging from 2 to 30 MPa, and approximated an exponential function ratio between thermal contact resistance and contact pressure. Shojaefard (2008) studied heat transfer between stainless steel and aluminum based on steady-state experiments. Blaise (2013) analyzed the changes in thermal contact resistance of USIBOR 1500P steel during hot stamping. In recent years, there have been increasing applications of boron steel in hot-stamping and, consequently, studies of the factors influencing the IHTC during forming and subsequent tempering have increased. For example, Hu (2013) studied the effect of oxide fouling on IHTC for 22MnB5 boron steel.

Figure 2

Process parameters that influence the properties of materials.

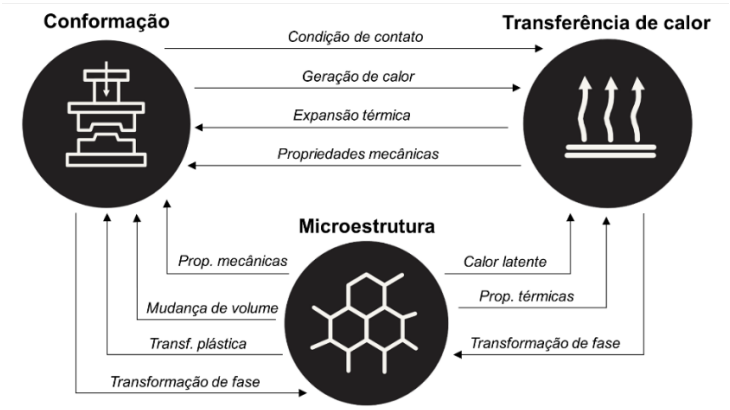

This work focused on reviewing models provided in the international literature for determining the IHTC. The paper consists of a theoretical review on the main heat transfer mechanisms during the hot stamping processes, focusing on the determination of the IHTC, followed by a discussion and a proposed model governing the overall heat transfer for the *Hot Stamping* process (Zhao, 2015).

2 THEORETICAL REFERENCE

2.1 HEAT TRANSFER DURING THE HOT STAMPING PROCESS STEPS

The hot-stamping process can be separated into two methods: direct (a) and indirect (b). Grouped in four steps, these steps include austenitization of the blank at 950 ºC in an oven, transfer of the generator to the matrices, conformation and tempering in a closed tool, as shown in figure 3.

Figure 3

Direct (a) and indirect (b) hot-stamping process.

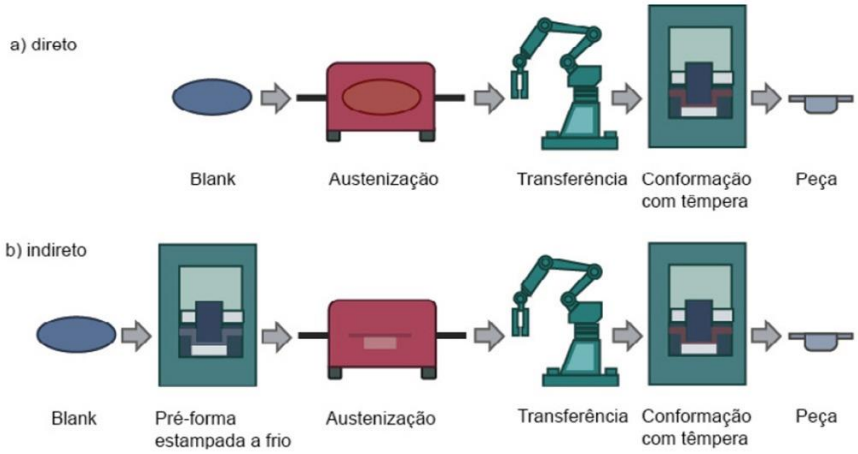

Source: Turetta, 2006.

To study heat transfer during the hot stamping process, it is necessary to analyze the steps in which heat is lost from the blank, which can be seen in Figure 4. The temperature in the part is assumed to be uniform due to its small thickness (0.6 - 3mm). Therefore, the rate of heat loss of the blank *Q(t)* can usually be expressed by equation 1.

Figure 4

Main heat transfer mechanisms.

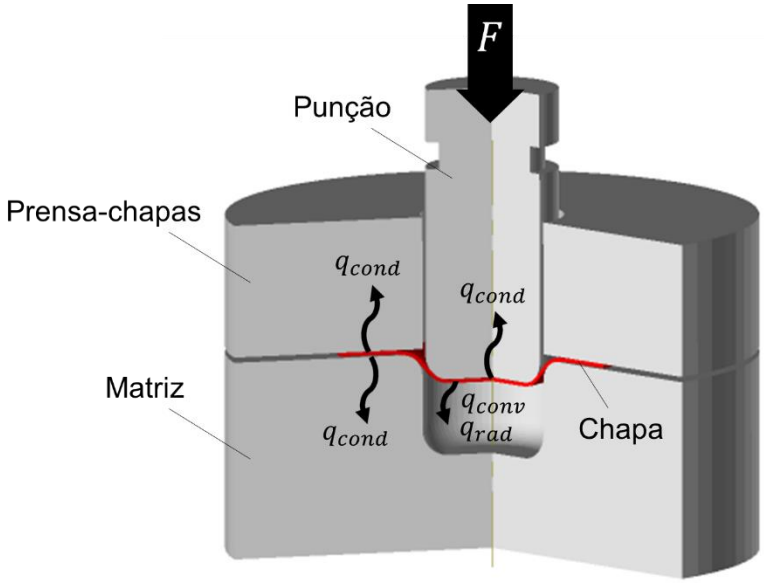

$$\dot{Q}\ (t) = mC_b\ \frac{dT_b}{dt} \qquad (1)\ (2)$$

During the hot-stamping process, the blank loses heat when it is transferred from the austenitization furnace to the forming tool (Q *tran.)*, when it is placed in the die *(Qsimplyplac.) and when it is in contact with the forming tools during the deformation and quenching phases (Qform.).* The heat lost by the part during the above mentioned phases *(total Q)*is considered negative, since the heat is released from the generator and can be expressed mathematically by equation 2.

$$\dot{Q}_{total}\ =\ -\ \dot{Q}_{tran.} - \dot{Q}_{plac.} - \dot{Q}_{form.} \qquad (1)$$

2.2 TRANSFER STAGE

During the transfer of the furnace to the stamping tools, the generator loses heat by radiation and convection to the surrounding air at atmospheric temperature (Shapiro, 2009; Abdulhay, 2011). Therefore, the heat loss of the blank at a given time is in the form of convective heat *Qconv.1* and radiative heat *Qrad.1*, as shown in equation 3.

$$\dot{Q}_{tran.=}\ \dot{Q}_{conv._1} + \dot{Q}_{rad._1} \qquad (3)$$

The hot generator is assumed to be transferred from the furnace to the forming tool in its horizontal position. To determine convective heat transfer during the transfer phase, the generator can be treated as a flat plate that loses heat on both sides by convection to ambient air (Shapiro, 2009; Liu, 2011; Liu, 2013), as shown in figure 5.

Figure 5

Heat loss of the part on the upper and lower surfaces.

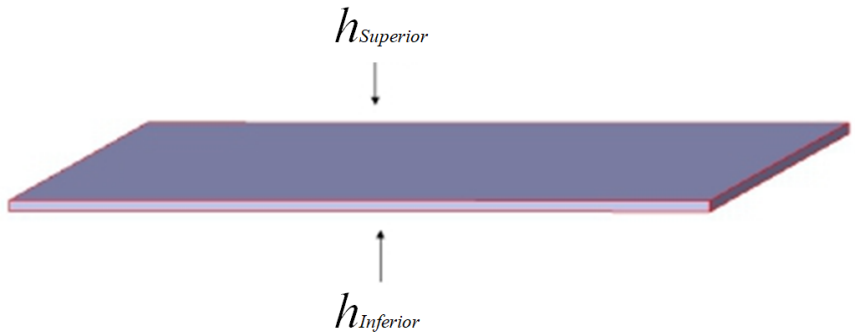

Source: Muvunzi (2017).

A small number of *Biot (Bi* <<1) is assumed for the blank due to its small thickness (0.6 - 3mm), high thermal conductivity (32 W/m.K) and large ratio between surface area and volume, which translates into a low characteristic length (Shapiro, 2009; Liu, 2011).

In addition, other literature authors have also confirmed a small number of *Biot* for the blank (Caron, 2013; Zhao, 2015). Based on this notion, the blank is considered to have uniform temperature during the transfer phase. The *Biot* number can be expressed using equation 4.

$$Bi = \frac{hL}{k} \qquad (4)$$

It can also be assumed that the heat lost at the edges of the blank is insignificant due to its small thickness (Abdulhay, 2011). According to the process requirements, the blank should be transferred to the forming tool shortly after being released from the furnace (Abdulhay, 2011). The effect of natural convection should be considered dependent on the process configuration. If rapid material handling devices, such as robotic arms, are used to quickly transfer the generator to the furnace, the effect of natural convection may be neglected or replaced. On the other hand, if the blank is left some time before the stamping stage, it is necessary to include the effect of the resulting natural convection. To re-examine these effects, preference is given to including the effect of natural convection in a detailed analysis.

Therefore, the total heat loss by convection on both sides of a hot flat plate is given by equation 5 (Hagen, 1999).

$$\dot{Q}_{conv.1} = A_b\,(h_{top} + h_{bot})(T_b - T_{air}) \quad (5)$$

The natural coefficients of upper and lower convection heat transfer can be calculated using equations 6 and 7 (Shapiro, 2009; Liu, 2011). The *Grashof* numbers (*Gr*) and the Prandtl(Pr) can be defined by equations 8 and 9.

$$h_{Superior} = [0{,}27(GrPr)^{0{,}33}]\frac{k_b}{L} \quad (6)$$

$$h_{Iferior} = [0{,}14(GrPr)^{0{,}25}]\frac{k_b}{L} \quad (7)$$

$$Gr = \frac{g\beta\rho^2(T_a - T_{bi})L^2}{\mu} \quad (8)$$

$$Pr = \frac{c_{b\mu}}{k} \quad (9)$$

Regarding equations 6 and 7, the convection heat transfer coefficient at the upper surface is higher than at the lower surface due to the effects of buoyancy (Çengel, 2015). Replacing equations 6 and 7 in equation 5 will result in equation 10:

$$\dot{Q}_{conv.1} = \frac{k_b}{L} A_b\,[0{,}27\,(GrPr)^{0{,}33} + 0{,}14\,(GrPr)^{0{,}25}]\,(T_{b-T_{air}}) \quad (10)$$

The radiative heat transfer from blank ($Q_{rad.}$) to the surfaces surrounding the floor and ceiling of the plant plant can be expressed by equation 10 (Hagen, 1999). For equation 11, a unit form factor has been applied.

$$\dot{Q}_{rad} = \sigma\,\varepsilon\,A_b\,(T_b^4 - T_{fac}^4) \quad (11)$$

It was mentioned earlier that the generator loses heat on both sides, as shown in figure 5. Thus, the heat lost in equation 11 is doubled, as shown in equation 12.

$$\dot{Q}_{rad.1} = 2\,\sigma\,\varepsilon\,A_b\,(T_b^4 - T_{fac}^4) \quad (12)$$

A single equation for the transfer phase can then be reformulated based on equation 3. This equation is obtained by replacing equations 10 and 12 in equation 13, as shown below.

$$\dot{Q}_{tran.} = \frac{k_b}{L} A_b \left[0{,}27\ (GrPr)^{0{,}33} + 0{,}14\ (GrPr)^{0{,}25}\right] \left(T_{b-T_{air}}\right) + 2\ \sigma\ \varepsilon\ A_b \left(T_b^4 - T_{fac}^4\right) \quad (13)$$

2.3 ALLOTMENT PHASE

The placement phase corresponds to the stage where the generator is placed between the punch and the matrix before conformation occurs, as shown in figure 6.

Figure 6

Transfer of plates to hot-stamping.

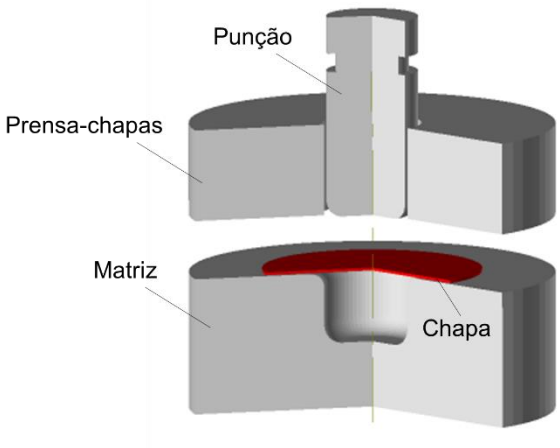

During the placement phase, the top surface of the blank is cooled by natural convection through the ambient air and by heat exchange by radiation with the punch and the sheet press. The lower surface can be divided into three sections. Two of the sections are cooled by thermal contact with the die surface. To effectively cool the generator, cooling channels are inserted into the die and punch. Therefore, it is presumed that the puncture and the matrix are at a lower temperature than that of the generator. The other section is at the top of the matrix cavity and is cooled by natural convection with air and heat exchange by radiation with the matrix (Abdulhay, 2011). This can be expressed using equation 14.

$$\dot{Q}_{plac.} = \left(\left(\dot{Q}_{conv.2} + \dot{Q}_{rad.2}\right) + \left(\dot{Q}_{con.1} + \dot{Q}_{conv.3} + \dot{Q}_{rad.3}\right)\right) \quad (14)$$

Heat lost by natural convection with ambient air at the top of the blank can be expressed by equation 15 (Hagen, 1999).

$$\dot{Q}_{conv.2} = Ah_{sup.}\,(T_b - T_{ar}) \qquad (15)$$

The punch and the plate-press are assumed to be at the same initial temperature. Therefore, the radiated heat transfer from the part to the punch and the plate press can be expressed using the usual expression of radiated heat transfer shown in equation 16 (Çengel, 2015). It is considered the radiation form factor (f_1) between the upper surface area of the blank and the lower surface area of the puncture and the sheet press. The surface area of the blank, which is exposed to the puncture and the press-plate (A_{bp}) is also considered.

$$\dot{Q}_{rad.2} = \sigma\varepsilon A_{bp} f_1 \left(T_b^4 - T_p^4\right) \qquad (16)$$

The IHTC at the interface between the generator and the matrix during placement (R_{plac}) is affected by surface area, lubrication conditions and contact surface integrity (Chang, 2016). Figure 7 shows that heat transfer occurs at certain points and this reduces the total area of contact, thus affecting the IHTC.

Figure 7

Surface topography at the contact interface between the part and the matrix

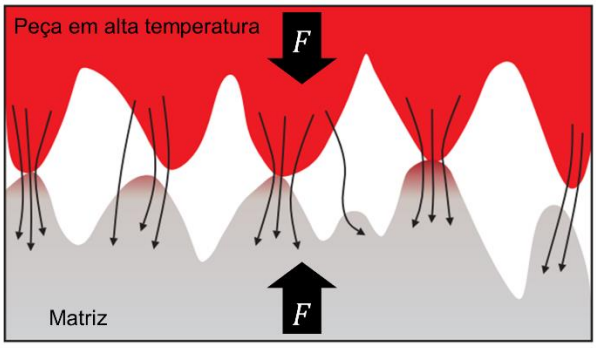

Equation 17 shows heat transfer at the interface between the blank and the matrix. The blank surface area in contact with the matrix (A_{bd1}) is again considered.

$$\dot{Q}_{con.1} = R_{plac} A_{bd1}\,(T_b - T_d) \qquad (17)$$

Heat loss by natural convection between the blank and the air space in the matrix cavity can again be expressed by equation 18.

$$\dot{Q}_{conv.3} = h_{bot2} A_{bd2} (T_b - T_{ar}) \quad (18)$$

It should be noted that the plate position in the matrix may limit the amount of heat transfer by convection, depending on the process configuration. Equation 19 shows radiative heat transfer between sheet metal and cavity. The liquid radiation form factor (f_2) between the bottom and sides of the cavity and the bottom of the blank is considered. A_{bd2} represents the surface area of the generator under the matrix cavity.

$$\dot{Q}_{rad.3} = \sigma \varepsilon A_{bd2} f_2 (T_b^4 - T_d^4) \quad (19)$$

The total heat lost by the blank during the approach phase can be expressed by equation 20, which is obtained by replacing equations 15, 16, 17, 18 and 19 in equation 14.

$$\dot{Q}_{plac.} = \left[A h_{sup.} (T_b - T_{ar}) + \sigma \varepsilon A_{bp} f_1 \left(T_b^4 - T_p^4\right)\right] + \left[R_{plac} A_{bd1} (T_b - T_d) + h_{bot2} A_{bd2} (T_b - T_{ar}) + \sigma \varepsilon A_{bd2} f_2 (T_b^4 - T_d^4)\right] \quad (20)$$

2.4 DEFORMATION AND TEMPERING STAGE

Deformation and tempering are assumed to occur simultaneously. During the forming and tempering phase, heat transfer occurs by contact between the hot part and the cold tool. Figure 8 shows the interfaces during deformation and tempering. The deformation of the plate in the matrix cavity causes its sliding in the zone of the plate press. However, the heat conduction to the sheet metal press during the deformation stage was considered insignificant due to the short slip time interval of the sheet metal and the relatively low contact pressure (Abdulhay, 2011).

Figure 8

Interface during stamping and seasoning.

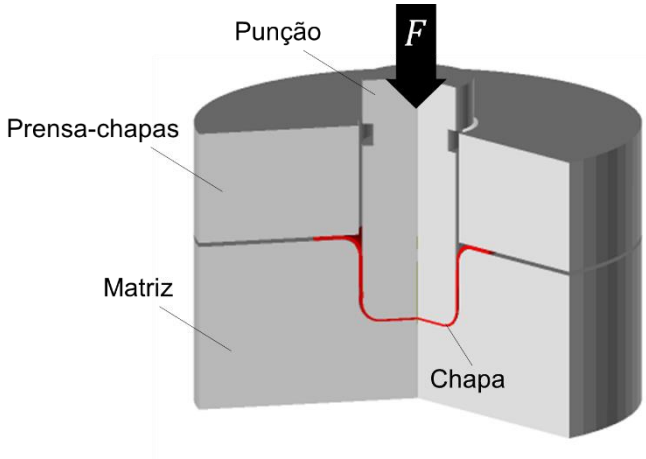

It is also assumed that the heat lost to the environment is negligible, since puncture and matrix temperatures are controlled by the cooling fluid over time. After the forming step, the blank is kept in the closed tool to allow cooling for about 15 to 25s (Steinbeiss, 2007).

2.4.1 General

The following heat transfer rates were considered for the conformation and tempering phases (Steinbeiss, 2007; Abdulhay, 2011):

- heat absorbed by the blank surface puncture ($\dot{Q}_1$);
- heat absorbed by the matrix from the surface of the generator ($\dot{Q}_2$);
- heat transferred from the matrix surface to the internal walls of the matrix cooling channel ($\dot{Q}_3$);
- heat transfer from the internal walls of the cooling channel from the matrix to the refrigerant ($\dot{Q}_4$);
- heat transported by the coolant in the cooling channels of the matrix ($\dot{Q}_5$);
- rate of work performed at blank as a result of friction forces ($\dot{W}_1$);
- rate of work performed in the blank due to plastic deformation ($\dot{W}_2$);
- heat released from sheet metal due to metallurgical transformations (assuming this is an exothermic reaction) ($\dot{Q}_6$).

The temperature of the plate changes as a function of the heat coming from the work carried out due to the forces of friction, plastic deformation ($\dot{W}_2$), *heat* released during the transformation of phases ($\dot{Q}_6$), heat absorbed by the matrix ($\dot{Q}_2$)*and by the puncture* ($\dot{Q}_1$).

Therefore, the sum of heat transfer and working rates during conformation can be expressed as shown in equation 21.

$$\dot{Q}_{form} = (\dot{Q}_1 + \dot{Q}_2) - (\dot{W}_1 + \dot{W}_2 + \dot{Q}_6) \quad (21)$$

The amount of heat transferred from the part to the tool depends on the design of the tool, the surface area, and the geometry of the final part. For simplicity, any transient thermal differences between the water-cooled puncture and die are ignored. Therefore, the following discussion focuses only on the data. The transients within the matrix are accounted for through the IHTC discussed below. The heat lost by the tool to the environment is considered negligible. Therefore, it is suggested that the heat transferred from the surface of the matrix to the walls of the cooling channel ($\dot{Q}_3$) is considered equivalent to the heat transferred from the walls of the cooling channel to the refrigerant ($\dot{Q}_4$) and to the heat transported by the refrigerant in motion ($\dot{Q}_5$) (Bai, 2012; Ghiotti, 2016) as shown in equation 22.

$$\dot{Q}_1 = \dot{Q}_2 = \dot{Q}_3 = \dot{Q}_4 = \dot{Q}_5 \quad (22)$$

2.4.1.1 Heat Transfer from Part Surface Interface to Matrix Surface

Heat is transferred from the part surface to the punch/matrix surface upon contact. It is assumed that the puncture and matrix are maintained at the same temperature and that heat is distributed evenly between them. The heat transfer from the surface of the generator to the matrix surface is defined by equation 23 (Ji, 2015).

$$\dot{Q}_2 = R_{form} A_b (T_b - T_d) \quad (23)$$

To analyze heat transfer during forming and tempering phases, it is necessary to determine the IHTC between blank and matrix/puncture (Li, 2015). The IHTC is an important parameter because it determines the time of deformation and tempering (Ji, 2015). The IHTC is also needed to perform an accurate analysis of finite elements of the hot stamping process (Caron, 2013). In addition, it can be used to determine the effect of other process parameters (pressure, temperature and surface roughness) on heat transferability. Therefore, the following section provides an overview and analysis of the methods that have been developed to determine the IHTC between the matrix/puncture and the blank.

2.4.1.2 Reverse Heat Conduction Analysis

One of the methods that has been used involves using reverse heat conduction analysis to obtain the heat flux between the blank and the matrix and use it to calculate the IHTC (Bai, 2012; Caron, 2014; Li, 2015; Zhao, 2015). The method is based on equation 24.

$$\frac{\dot{Q}}{A} = R_{form}\left(T_{b\,(t)} - T_{d\,(t)}\right) \qquad (24)$$

The temperature values Tb(*t*) and Td(t) and the heat $\left(\frac{\dot{Q}}{A}\right)$ flux are pre-determined to obtain the IHTC. Heat flow is obtained using the Fourier conduction law, as shown in equation 25 (Hu, 2013).

$$\frac{\dot{Q}}{A} = -k_{bd}\frac{dT_{bd}}{dx} \qquad (25)$$

The limitation of the method is due to the challenge of measuring the temperature of the sheet metal and the matrix during the operation of forming and tempering. Bai *et al* (2012) have developed a numerical procedure to determine the temperature at specific locations of a part and matrix in a turbine blade forging process. Physical measurements were also made with thermocouples at the specified locations. The heat flux was then calculated to obtain the IHTC (3.5 kW/m^2.K). To validate the developed procedure, the IHTC calculated on a Finite Element model with conditions similar to the experiment was used. The results showed that the temperature values obtained in the FE simulation were very close to the numerical procedure. Li *et al.* (2015) used the inverse heat analysis technique to develop a model for the IHTC as a power function of contact pressure, which was evaluated using Finite Element analysis. The model was tested to predict phase transformation from a blank to hot stamping. According to the results, a proportion of martensitic phase of 87% was obtained in the experiments and 84% was obtained in the Finite Element Analysis. Li *et al.* (2015) developed software for calculating IHTC between a hot stamping matrix and a blank using reverse heat conduction analysis. The software was used to determine the effect of the matrix surface temperature and contact pressure on the IHTC. According to the results, the IHTC (W/m^2.K) for different pressure values of 1, 10, 20 and 40 MPa led to the derivation of a linear function. The blank surface temperature was found not to have a significant effect on the IHTC (Li, 2015).

2.4.1.3 Newton's Cooling Law

Newton's law of cooling can be used to determine the IHTC (Merklein 2009; Bosetti, 2010; Caron, 2014; Ji, 2015; Gu, 2016). This method is based on equation 26.

$$T_{b(t)} = (T_{bo} - T_{di})e^{\frac{-R_{form}A_b t}{\rho V C_b}} + T_{di} \quad (26)$$

Making R_{form} the subject of the equation results in equation 27 [34].

$$R_{form} = \frac{-\rho V C_b}{A_b t} \ln\left[\frac{T_{b(t)} - T_{di}}{T_{bo} - T_{di}}\right] \quad (27)$$

Other parameters of the equation can then be identified and used for the calculation of the IHTC. Temperature values can be measured using integrated blank and matrix thermocouples (Huang, 2016). Merklein *et al.* (Merklein, 2009) studied the thermal behavior of custom blanks, analyzing the effect of a constant IHTC at different tool temperatures (between 20 and 300 K), pressure and clearance between blank and matrix. In the study, Newton's law of cooling was used in the calculation of the IHTC and resistive heating cartridges were used to control the temperature of the matrix. However, the challenge of assuming constant ambient temperature was a model limitation, since heat transferred by the generator to the tool results in a change in the tool temperature. Huang *et al.* (2016) used Newton's law of cooling to investigate the effect of contact pressure on IHTC during hot stamping. A Finite Element analysis model was also developed using Abaqus (2015) to evaluate the results. According to the results, the IHTC increased from 1764 to 3782 W/m^2.K with an increase in pressure from 0 to 30 MPa. However, comparing the two models, the FE model gave more accurate results and proved that the IHTC changed over time, unlike Newton's law of cooling, which gave a constant value. Bosetti *et al.* (2010) also carried out a similar study to investigate the effect of contact pressure on the IHTC under similar conditions as industry. Two approaches were used, namely Newton's law of cooling and inverse analysis of heat conduction. Both approaches have shown that contact pressure directly affects the IHTC. However, the challenge of the study lies in the large deviation between the IHTC values obtained for the same pressure. For example, a contact pressure of 5 MPa resulted in an IHTC of 1000 W/m^{2}K using inverse heat conduction analysis and 1231 W/m^{2}K using Newton's law of cooling.

2.4.1.4 Heat Balance Method

Zhao *et al.* (2015) modified Newton's law of cooling model to meet the change in tool temperature and called it the heat balance method. The heat balance method is based on the assumption that all heat lost by the plate is absorbed by the matrix and the puncture (energy conservation law). When developing the model, the authors considered only the transfer of heat to the matrix. Equation 28 can be used to mathematically describe the method.

$$C_b \rho V \frac{dT_b}{dt} = -R_{fom} A_b (T_b - T_d) \qquad (28)$$

Regarding equation 28, the left side represents the variation of the internal energy of the generator and the right side shows the heat transfer from the blank to the matrix. As the tool temperature varies during forming and tempering processes, equation 28 can be integrated to produce equation 29.

$$\int_{T_{bo}}^{T_{bi}} dT_b = -\frac{R_{form} A_b}{c_b \rho V} \int_{t_o}^{t_i} (T_b - T_d)\, dt \qquad (29)$$

Unlike Newton's law of cooling, the tool temperature (T_d) changes over time. The equation can be solved using the trapezoidal rule, as shown in Figure 9, since both the puncture and matrix temperatures vary linearly with time. When the area under the graph is determined using the trapezoid rule, equation 30 is given origin.

$$T_{bi} - T_{bi} = -\frac{R_{form} A_b}{c_b \rho V} * \frac{1}{2} [(T_{bo} - T_{do}) + (T_{bi} - T_{di})] * (t_i - t_o) \qquad (30)$$

Figure 9

Area below temperature chart.

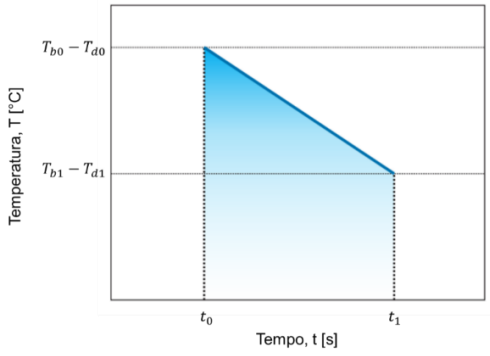

Source: Zhao *et al.* (2015).

The time difference of t_0 to ti^1*becomes the cooling time, equation 31, of the generatrix.*

$$T_{bi} - T_{bo} = -\frac{R_{form}A_b}{2c_b\rho V}[(T_{bo} - T_{do}) + (T_{bi} - T_{di})]t \quad (31)$$

Rearranging equation 31 and making R_{form} the subject will result in equation 32. The V volume and the area A are divided to provide the characteristic thickness, y, of the part.

$$R_{form} = \frac{2c_b\rho y\,(T_{bo} - T_{bi})}{[(T_{bi} - T_{di}) + T_{bo} - T_{do}]t} \quad (32)$$

Again, it is assumed that half of the heat lost by the part is transferred to the puncture and the other half is transferred to the matrix. Thus, half the thickness of the piece is considered the characteristic thickness. According to Zhao *et al.* (2015), experimental analysis shows that equation 29 provides a good prediction of the IHTC at the beginning and end of the tempering process. In the study, Zhao *et al.* (2015) compared the accuracy of the reverse heat conduction analysis, heat balance and optimization method. Experimental devices were used to collect data on the surface and internal temperature of the sheet and matrix. The accuracy of the methods was evaluated based on a simulation of Finite Elements of the experiment. According to the results, the inverse heat conduction analysis presented an error of 3.7%, the heat balance method presented an error of 7.5% and the optimization method had an error of 10.3%. Ying *et al* (2017) compared the accuracy of the reverse heat conduction analysis and the heat balance method during hot forming of an aluminum alloy 7075-T6. Average error rates of 3.08 and 4.4% were obtained using the inverse heat conduction analysis, while the heat balance method resulted in 14.79 and 4.48%. Consequently, the analysis of inverse heat conduction proved more accurate when compared to the heat balance method.

2.4.2 Heat Transfer from Matrix Surface to Cooling Channel Wall

Heat transferred from the matrix surface to the cooling channel walls can be illustrated by Figure 10.

Figure 10

Heat transfer from matrix surface.

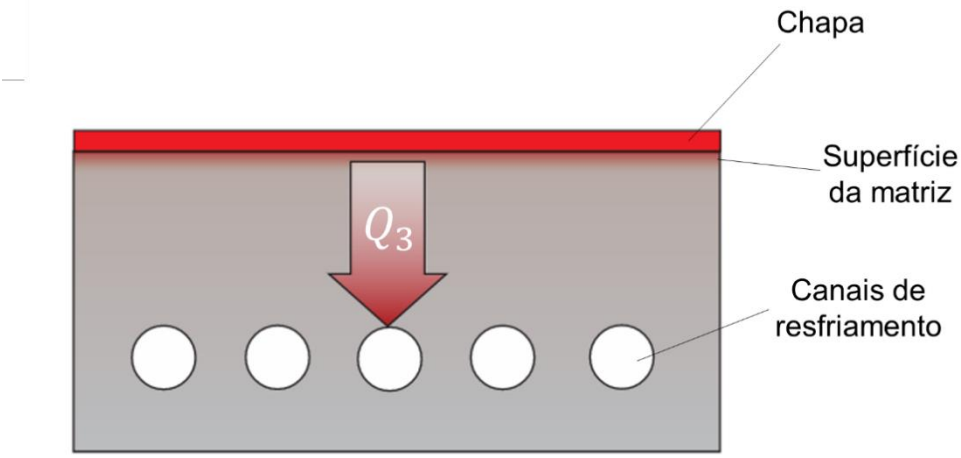

To determine the amount of heat transferred, conduction form factor analysis can be used (Ji, 2015). This is shown in equation 33.

$$\dot{Q}_3 = k_d f_3 \, (T_d - T_{cw}) \qquad (33)$$

Assuming the matrix is flat, the form factor (f_3) can be defined by equation 34 (Ji, 2015).

$$f_3 = \frac{2\pi l}{\ln\left[\left(\frac{2w}{\pi d}\right)\sin(h_w)\left(\frac{2\pi Zb}{w}\right)\right]} \qquad (34)$$

The replacement of equation 34 in equation 33 will result in equation 35:

$$\dot{Q}_3 = k_d \frac{2\pi l}{\ln\left[\left(\frac{2w}{\pi d}\right)\sin h_w \left(\frac{2\pi Zb}{w}\right)\right]} \, (T_d - T_{cw}) \qquad (35)$$

For a given number of cooling channels *n*, the total heat transferred from the matrix surface to the cooling channels, equation 36 is used:

$$\dot{Q}_3 = nk_d \frac{2\pi l}{\ln\left[\left(\frac{2w}{\pi d}\right)\sin h_w \left(\frac{2\pi Zb}{w}\right)\right]} \, (T_d - T_{cw}) \qquad (36)$$

To increase heat transfer between the die surface and the cooling channel wall, the number of cooling channels can be increased. Another way is to improve the design of the

cooling channels so as to increase the value of ($_{fs}$). On the other hand, the use of materials in tools with better thermal conductivity also helps to increase heat transfer (Karbasian, 2010).

2.4.3 Heat Transfer from Cooling Channel Walls to Coolant Fluid

Equation 37 can be used to determine the heat lost from the wall of the cooling channel to the refrigerant.

$$\dot{Q}_4 = h_w A_{cw} (T_{cw} - T_w) \quad (37)$$

The surface area of the channels ($_{Acw}$) can be defined by equation 38.

$$A_{cw} = \pi d l \quad (38)$$

The convection heat transfer coefficient can be obtained using the *Nusselt* number, as shown in equation 39.

$$h_w = \frac{Nuk_w}{d} \quad (39)$$

If equations 38 and 39 are replaced in equation 37, the total heat transfer from the cooling channel walls to the refrigerant for a given number of cooling channels η becomes (equation 40):

$$\dot{Q}_4 = nNuk_w \pi l (T_{cw} - T_w) \quad (40)$$

To improve heat transfer between the walls of the cooling channel and the coolant, the diameter of the cooling channels and the coolant speed can be increased to increase the *Nu* value. However, the effect of the yield strength of the material must be taken into account to avoid plastic deformation of the tool.

2.4.4 Heat Transported by Coolant Fluid in Channels

The rate of heat removal by water in the cooling channels is defined by equation 41 (Hosford, 2011).

$$\dot{Q}_5 = \dot{m}C_w\left(T_{fora} - T_{dentro}\right) \quad (41)$$

2.4.5 Thermal Balance between Tool Surface and Coolant

Equation 42 was proposed for the energy balance during the formation and tempering phase.

$$nk_d \frac{2\pi l}{\ln\left[\left(\frac{2w}{\pi d}\right)\sin h_w\left(\frac{2\pi Zb}{w}\right)\right]}\left(T_d - T_{cw}\right) = nNuk_w\pi l\left(T_c - T_w\right) = \dot{Q}_5 = \dot{m}C_w\left(T_{fora} - T_{dentro}\right) \quad (42)$$

2.4.6 Rate of Work Performed Due to Friction and Plastic Deformation

The rate of work performed due to friction depends on the normal contact force *(F_1)* and the slip velocity ($v1$), as shown in equation 43 (Van Der Heide, 2002).

$$\dot{W}_1 = \eta F_1 v_1 \quad (43)$$

Equation 44 describes the rate of work done during plastic deformation (Kapoor, 1998; Hosford, 2011).

$$\dot{W}_2 = \lambda V \int_0^{\epsilon} mEU/t \quad (44)$$

The fraction for martensitic transformation *U* is given by the *Koistinen-Marbuger* law as shown in equation 45, where α represents the voltage-dependent transformation constant and T_{ms} is the initial temperature of the martensitic transformation (Gu, 2016).

$$U = 1 - e^{-\alpha\left(T_{ms} - T_b\right)} \quad (45)$$

Replacing equation 45 in equation 44 results in:

$$\dot{Q}_6 = \frac{mE\left(1 - e^{-\alpha\left(T_{ms} - T_b\right)}\right)}{t} \quad (46)$$

For a typical 22MnB5 steel, the values of *E* (latent heat), α andTms are 85 kJ/kg, 3.02577 K, and 411.3 K, respectively (Gu, 2016).

2.4.7 Equation for Heat Transfer During Formation

The rate of heat transfer at the conformation stage is described by equation 47, based on the assumption that the puncture and matrix absorb heat in equal parts during the conformation and tempering phases ($Q_t = Q_2$).

$$\dot{Q}_{form} = 2R_{form}A_b(T_b - T_d) - \left[\eta F_1 v_1 + mE\frac{\left(1 - e^{-\alpha(T_{ms} - T_b)}\right)}{t + \lambda V \int_0^{\epsilon} \tau d\,\epsilon}\right] \quad (47)$$

3 DISCUSSION

During the transfer phase, the heat loss of the generator mainly depends on its surface area and the method by which it is transferred from the furnace to the stamping tools. Depending on the configuration of the process, forced convection may need to be considered. In relation to the positioning stage, the geometry of the tool and the speed of the press are of great importance. For the forming phase, the surface area, roughness, material properties and temperature of the contact surfaces have a major influence on heat transfer.

Some of the models for determining the IHTC use direct temperature measurements. The challenge of this practice is that it is difficult to obtain accurate readings of thermocouples, since temperatures change rapidly and the response time of thermocouples needs to be considered. Thermocouples are also exposed to high-pressure conditions and this can also have a negative effect on the resulting readings. On the other hand, the use of FEM requires the input of several process parameters and also involves many iterations. Analysis of the literature revealed that reverse heat conduction analysis is the most accurate method and the FEM-based method is the least accurate method for calculating the IHTC. Based on the analysis performed, equation 48 is proposed for global heat transfer.

$$\dot{Q}_{total} = -\left[\frac{k_b}{L} A_b\,[0{,}27\,(GrPr)^{0{,}33} + 0{,}14\,(GrPr)^{0{,}25}\,](T_b - T_{ar}) + 2\sigma\varepsilon A_b\left(T_b^4 - T_{fac}^4\right)\right] - \left[\left(Ah_{sup.}\,(T_b - T_{ar}) + \sigma\varepsilon A_{bp} f_1\left(T_b^4 - T_p^4\right)\right) + R_{plac}A_{db1}\,(T_b - T_d) + h_{bot2}A_{db2}\,(T_b - T_{ar}) + \sigma\varepsilon A_{db2} f_2(T_b^4 - T_d^4)\right] - \left[2R_{form}A_b\,(T_b - T_d) - \left(\eta F_1 v_1 + mE\frac{\left(1 - e^{-\alpha(T_{ms} - T_b)}\right)}{t + \lambda V \int_0^{\epsilon} \tau\, d\epsilon}\right)\right] \quad (48)$$

The proposed equation is useful in identifying critical parameters, which can be used for effective thermal management of the hot-stamping process. Effective thermal management

in hot stamping is required to reduce blank cooling time, resulting in reduced cycle time, ultimately leading to improved productivity and reduced production costs.

4 CONCLUSION

The purpose of the article was to present a review on the heat transfer models during the hot stamping process, provided for in the international literature. The next stage of this research, the object of study of two doctorate theses, will involve the validation of the proposed models. This can be achieved by conducting experiments and simulating the hot-stamping process. To gain more insight into heat transfer during the quenching phase, there is need for further studies on the design of the cooling system. It is necessary to examine the effect of refrigeration system parameters on heat transfer.

ACKNOWLEDGEMENTS

The authors thank the Federal University of Rio Grande do Sul (UFRGS) for the infrastructure for carrying out the experimental trials, as well as the National Council for Scientific and Technological Development (CNPq) for the concession of grants that foster the development of national scientific research, through Processes 309188/2021-0, 446930/2023-7 and 408298/2023-5.

REFERENCES

Abdulhay, B., *et al.* (2011) Development of Estimation Procedure of Contact Heat Transfer Coefficient at the Part-tool Interface in Hot Stamping Process. *Heat Transfer Engineering.* Vol. 32(6). P. 497-505.

Abdulhay, B., Bourouga, B., Dessain, C. (2011) Experimental and Theoretical Study of Thermal Aspects of the Hot Stamping Process. *Applied Thermal Engineer-ing.* Vol. 31(5). P. 674-685.

Abdulhay, B., Bourouga, B., Dessain, C., (2012) Thermal Contact Resistance Estimation: Influence of the Pressure Contact and the Coating Layer During a Hot Form-ing Process. *Int. J. Mater. Form.* Vol. 5 (3), P. 1–15.

Altan, T., Tekkeya, A. E. (2012) Sheet Metal Forming Processes and Applications, *ASM International.*

Arpaci, V. S., Selamet, A., Kao, S. (2000) *Introduction To Heat Transfer*, Upper Saddle River.

Bai, Q., *et al.* (2012) An Efficient Closed-form Method for Determining Interfacial Heat Transfer Coefficient in Metal Forming, International *Journal of Machine Tools Manufacture*. Vol. 56. P. 102-110.

Blaise, A., *et al.* (2013) Thermal Contact Resistance Estimation and Metallurgical Transformation Identification During the Hot Stamping. *Appl. Therm. Eng.* Vol. 61 (2) P.141–148.

Bosetti, P., *et al.* (2010) Interlaboratory Comparison for Heat Transfer Coefficient Identification in Hot Stamping of High Strength Steels. *International Journal of Materials Forming.* Vol. 3. P. 817-820.

Caron, E., Daun, K. J., Wells, M. A. (2013) Experimental Characterization of Heat Transfer Coefficients during Hot Forming Die Quenching of Boron Steel, *Metallurgical and Materials Transactions B.* Vol. 44(2). P. 332-343.

Caron, E. J., Daun, K. J., Wells, M. A. (2014) Experimental Heat Transfer Coefficient Measurements During Hot Forming Die Quenching of Boron Steel at High Temperatures. *International Journal of Heat and Mass Transfer.* Vol. 71. P. 396-404.

Chang, Y., *et al.* (2016) Investigation of the Factors Influencing the Interfacial Heat Transfer Coefficient in Hot Stamping. *Journal of Materials Processing Technology*. Vol. 228. P. 25–33.

Çengel, Y. A., Ghajar, A. J. (2015) *Heat and Mass Transfer: Fundamentals & Application*, 5th Edition in SI Units.

Escher, C., Wilzer, J. J. (2015) Tool Steels for Hot Stamping of High Strength Automo-tive Body Parts. *Proceedings of the International Conference of Stone Concrete Machining*. Vol. 3. P. 219-228.

Ghiotti, A., *et al.* (2016) Tribological Behavior of High Thermal Conductivity Steels for Hot Stamping Tools. *Tribology International*. Vol. 97. P. 412-422.

Gu, Z. W., *et al.* (2016) Heat Transfer Coefficient Evolution of Boron Steel during Hot Forming Die Quenching. *Material Science and Technology*. Vol. 32(2). P. 173-180.

Hagen, K. (1999) *Heat Transfer with Applications,* Prentice Hall, New Jersey,

Hosford, W. F., Caddell, R. M. (2011) *Metal Forming: Mechanics and Metallurgy*, 4th Edition, Cambridge University Press. London.

Hu, P., *et al.* (2013) Effect of Oxide Scale on Temperature-Dependent Interfacial Heat Transfer In Hot Stamping Process. *J. Mater. Process. Technol.* Vol. 213 (9). P.1475–1483.

Huang, R., *et al.* (2016) Energy and Emissions Saving Potential of Additive Manufacturing: The Case of Lightweight Aircraft Components. *Journal of Cleaner Production*. Vol. 135. P. 1559-1570.

Hung, T. H., *et al.* (2014) Measurement of Heat Transfer Coefficient of Boron Steel in Hot Stamping. *Procedia Engineering*. Vol. 81. P. 1750-1755.

Ikeuchi, K., Yanagimoto, J. (2011) Valuation Method For Effects Of Hot Stamping Process Parameters On Product Properties Using Hot Forming Simulator. J. *Mater. Process. Technol.* Vol. 211 (8). P. 1441–1447.

Ji, K., *et al.* (2015) Determination of Heat Transfer Coefficient for Hot Stamping Process. *Materials Today: Proceedings.* Vol. 2(2). p. 434 - 439.

Kapoor, R., Nemat-Nasser, S. (1998) Determination of Temperature Rise during High Strain Rate Deformation. *Mechanics of Materials*. Vol. 27(1). P. 1-12.

Karbasian, H., Tekkaya, A. E. A (2010) Review on Hot Stamping. *Journal of Material Processing Technology*. Vol. 210(15). P. 2103-2118.

Li, H., *et al.* (2015) Research on the Effect of Boundary Pressure on the Boundary Heat Trans-fer Coefficients between Hot Stamping Die and Boron Steel. *International Journal of Heat and Mass Transfer*. Vol. 91. P. 401-415.

Lim, W. S., *et al.* (2014) Cooling Channel Design of Hot Stamping Tools for Uniform High-strength Components in Hot Stamping Process. *International Journal of Advanced Manufacturing Technology*. Vol. 70(5-8). P.1189-1203.

Liu, H., *et al.* (2011) Numerical and Experimental Investigation into Hot Forming of Ultra High Strength Steel Sheet, *Journal of Materials Engineering and Performance*. Vol. 20(1). P. 1-10.

Liu, H., LEI, C., XING, Z. (2013) Cooling System of Hot Stamping of Quenchable Steel BR1500HS: Optimization and Manufacturing Methods. *International Journal of Advanced Manufacturing Technology*. Vol. 69(1-4). P. 211-223.

Merklein, M., Lechler, J., Stoehr, T. (2009) Investigations on the Thermal Behavior of Ultra High Strength Boron Manganese Steels within Hot Stamping, *International Journal of Material Forming*. Vol. 2(1). P. 259-262.

Muvunzi, R., *et al.* (2017) Heat Transfer in a Hot Stamping Process: A Review. *R&D j.* (Matieland, Online). Vol.33. Stellenbosch, Cape Town.

Nakagawa, Y., Maeno, T. Mori, K. I. (2015) Forming and Quenching Behaviors in Hot Stamping of Thin Quenchable Sheets. *MATEC Web of Conferences*.

Shan, Z. D., *et al.* (2010) Basic Study on Die Cooling System of Hot Stamping Process. *Proceedings of the International Conference of Advanced Technology Design Manufacturing*. P. 65-68.

Steinbeiss, H., *et al.* (2007) Method for Optimizing the Cooling Design of Hot Stamping Tools. *Production Engineering*. Vol.1(2). P. 149-155.

Shapiro, A. B. (2009) Using LS-Dyna for Hot Stamping. *Proceedings of the 7th European LS-DYNA Users Conference*, Salzburg, Austria,

Shojaefard, M. H., Goudarzi, K., (2008) The Numerical Estimation Of Thermal Con-tact Resistance In Contacting Surfaces. *Am. J. Appl. Sci.* Vol. 5 (11). P. 1566–1571.

Van Der Heide, E. (2002) *Lubricant Failure In Sheet Metal Forming*. Phd Thesis. Uni-versity of Twente.

Turetta, A., Bruschi, S., Ghiotti, A. (2006) Investigation of 22MnB5 Formability in Hot Stamping Operations. *J. Mater. Process. Technol.* Vol. 177 (1–3), P. 396–400.

Ying, X., Zhong-De, S. (2014) Design Parameter Investigation of Cooling Systems for UHSS Hot Stamping Dies. *International Journal of Advanced Manufacturing Technology*. Vol. 70(1-4). P. 257-262.

Ying, L., *et al*, (2017) Investigation of Interfacial Heat Transfer Mechanism for 7075-T6 Aluminum Alloy in HFQ Hot Forming Process. *Applied Thermal Engineering.* Vol. 118. P. 266-282.

Zamri, M. F., Yusoff, A. R. (2015) Optimization of Cooling Channel Design in the Hot Stamping Die for Hot Stamping Process. *Advances in Materials and Processing Technology*. Vol. 1(1-2). P. 27-35.

Zhao K, *et al.* (2015) Comparison of the Methods for Calculating the Interfacial Heat Transfer Coefficient in Hot Stamping. *Applied Thermal Engineering.* Vol. 79. P. 17-26.

LIST OF SYMBOLS

A_b - Blank area [mm^2]

A_{cw} - Cooling channel wall area [mm^2]

A_{bp} - Area of the blank which is exposed to the puncture and to the plate press [mm^2]

A - Surface area [m^2]

A_b - Blank surface area [mm^2]

A_{bd1} - Blank surface area in contact with matrix [mm^2]

A_{bd2} - Blank surface area in contact with matrix (air space area in matrix cavity) [mm^2]

$\dot{Q}_1$ - Heat absorbed by blank surface puncture [J]

$\dot{Q}_2$ - Heat absorbed by the matrix from the surface of the generator [J]

$\dot{Q}_3$ - Heat transferred from the matrix surface to the internal walls of the matrix cooling channel [J]

$\dot{Q}_5$ - Heat transported by the coolant in the cooling channels of the matrix [J]

$\dot{Q}_6$ - Heat released from sheet metal due to metallurgical transformations (assuming that it is an exothermic reaction [J]

c - Specific heat capacity [J/kg.K]

C_b - Specific heat capacity blank [J/kgK]

h_{bot} - Lower convective heat transfer coefficient of the plate [W/m^{2}K]

h_{sup} - Upper convective heat transfer coefficient of the plate [W/m^{2}K]

R - Interfacial heat transfer coefficient [W/m^{2}K]

R_{plac} - Interfacial heat transfer coefficient (in the placement phase) [W/m^{2}K]

R_{form} - Interfacial heat transfer coefficient (Phase Transformation) [-]

h - Heat transfer coefficient by convection [W/m^{2}K]

h_{bot2} - Coefficient of heat transfer by lower convection of the plate (area of air space in the matrix cavity) [W/m^{2}K]

h_w - Convective heat transfer coefficient (channel coolant) [W/m^{2}K]

l - Cooling channel length [m]

k - Thermal [W/m.K]

k_d - Matrix thermal conductivity [W/m.K]

x - Thermal conduction direction [mm]

d - Cooling channel diameter [mm]

w - Center distance of cooling channels [mm]

Z_b - Distance from center of cooling channel to surface of blank [mm]

b - Distance from the surface to the center of the cooling channel [mm]

a - Distance between cooling channels [mm]

H - Hardness [N/m^2]

E - Latent thermal energy [J/kg]

L - Blank space length scale [m]

y - Thickness [mm]

g - Thickness of air gap [mm]

f - Form Factor [-]

f_1 - Radiation form factor (between the upper surface area of the blank and the lower surface area of the puncture and the sheet press) [-]

f_2 - Liquid radiation form factor between the bottom and sides of the cavity and the bottom of the blank [-]

f_3 - Form factor of the cooling channels of the matrix [-]

F - Force [N]

U - Martensite transformation fraction [%]

s - Inclination of surface roughness [μm]

m - Mass [kg]

Bi - Biot Number $Bi = \frac{hL}{k}$

n - Number of cooling channels

Gr - Grashof Number = $\frac{g\beta\rho^2(T_a - T_{bi})L^2}{\mu}$

Nu - Nusselt number [Nu = hD/k]

Pr - Prandtl Number [Pr = μo/k]

P - Pressure [MPa]

r - Radius of cooling channel [mm]

T - Temperature [ºC]

t - Time [s]

T_b - Blank temperature [ºC]

T_{air} - Ambient temperature [ºC]

T_{bi} - Initial blank temperature [ºC]

T_{fac} - Surface temperature [ºC]

T_p - Puncture temperature [ºC]

T_d - Matrix temperature [ºC]

T_{bo} - Final temperature of blank [ºC]

T_{di} - Initial matrix temperature [ºC]

T_{cw} - Cooling channel wall temperature [ºC]

T_w - Liquid coolant temperature [ºC]

T_{fora} - Non-matrix liquid temperature [ºC]

T_{dentro} - Temperature of the liquid within the matrix [ºC]

T_{ms} - Initial martensitic transformation temperature [ºC]

t - Time [s]

$\dot{Q}_4$ - Heat transfer from the internal walls of the cooling channel from the matrix to the refrigerant [J]

$\dot{Q}_{conv2}$ - Heat transfer by convection on the upper surface [W]

$\dot{Q}_{conv3}$ - Heat transfer by convection at the bottom surface [W]

$\dot{Q}_{total}$ - Total heat transfer [W]

$\dot{Q}_{tran.}$ - Transfer phase heat transfer [W]

$\dot{Q}_{plac.}$ - Heat transfer at instant blank contact with tool [W]

$\dot{Q}_{form.}$ - Heat transfer during plastic deformation and tempering [W]

$\dot{Q}_{conv._1}$ - Heat transfer by convection [W]

$\dot{Q}_{rad_1}$ - Radiation heat transfer [W]

$\dot{Q}$ (t) - Heat transfer rate [W]

$\dot{W}$ - Rate of work performed [W]

$\dot{W}_1$ - Work rate performed on blank as a result of friction forces [W]

$\dot{W}_2$ - Work rate performed on blank due to plastic deformation [W]

$\dot{Q}_{rad_1}$ - Radiation heat transfer rate (transfer phase) [W]

$\dot{Q}_{rad2}$ - Radiated heat transfer rate at the upper surface (placement phase) [W]

$\dot{Q}_{rad3}$ - Radiated heat transfer rate at the lower surface (placement phase) [W]

$\dot{m}$ - Mass flow rate [kg/s]

v - Speed [m/s]

V - Blank Volume [m^3]

Greek Symbols

α - Fraction of the plastic work carried out converted into heat

β - Volumetric expansion coefficient of the fluid [K^{-1}]

δ - Error function

ε - Emissivity of blank as a function of deflection velocity [s^{-1}]

λ - Material constant [K^{-1}]

μ - Viscosity [kg/s.m]

$_{ji}$ - Coefficient of friction

η - Standard deviation of surface roughness (*rad*)

ρ - Blank density [kg/m^3]

σ - **Stefan-Boltzmann** Constant [Wm^{-2K}

τ - Voltage [N/m^2]

Φ - Conductance [W/m^2K]